Advances in Technology Innovation, vol. 9, no. 4, 2024, pp. 273-286

Enhanced Design of On-Chip Monopole Antenna Inspired by Partially Reflective Surface at 5.8 GHz

Ahmadu Girgiri[1], Mohd Fadzil Ain[1,*], Mohd Zamir Bin Pakhuruddin[2], Bello Abdullahi Muhammad[1], Abdullahi Sarkin Bauchi Mohammed[1]

[1]School of Electrical and Electronic Engineering, University Sains Malaysia, Nibong Tebal, Malaysia

[2]School of Physic, University Sains Malaysia, Penang, Malaysia

Received 24 April 2024; received in revised form 24 July 2024; accepted 25 July 2024

DOI: https://doi.org/10.46604/aiti.2024.14048

Abstract

The increasing popularity of compact, chip-based devices has spurred interest in developing on-chip antennas (OCAs). However, OCAs suffer from low gain and poor radiation efficiency due to the silicon substrate's low resistivity and high permittivity, influencing antenna performance. To avert these challenges, this study aims to enhance an OCA's gain and radiation efficiency by incorporating a partially reflective surface (PRS) into the antenna structure. The antenna is simulated using 3D CST software, and its performance is evaluated. To validate the simulation, an antenna prototype is fabricated using sputtering and chemical vapor deposition (CVD) technologies. The prototype demonstrates a peak gain of 2.14 dB and radiation efficiency of 72.2%, showing a 24.3% gain increase and a 16.25% efficiency increase compared to the design without PRS. Additionally, it achieves an impedance bandwidth of 0.63 GHz, making it suitable for WiMAX, RFIC, and Wi-Fi 6 applications.

Keywords: on-chip antenna, gain, partially reflective surface, radiation efficiency, silicon substrate

1. Introduction

In recent years, the demand for compact and integrated devices has risen due to the emergence of new applications. This increased demand has necessitated the development of integrated antennas, specifically on-chip antenna (OCA) technology. OCA is a noteworthy chip-based antenna that can be integrated into a silicon chip alongside other proximity radio frequency (RF) front-end components [1]. It is potentially integrated into Internet-of-things (IoT) based devices, energy harvesting, emerging wireless systems, and similar devices. Its applications span various devices such as mobile phones, transceivers, and IoT devices [2]; as a result, the need for communication channels that are low-power, secured, and high-speed has become essential. This facilitates the seamless integration of OCAs into compact transceivers in lower and higher applications [3-6].

Numerous studies highlight the potential and significance of integrated antennas in expansive settings. The prevalent approach involves either single-chip modules (SCM) or multi-chip modules (MCM) [7-9]. However, silicon as a substrate poses significant challenges due to its low resistivity and high permittivity [10-11]. These drawbacks adversely impact the antenna performance and distort its radiation and signal integrity [12-13]. To overcome these limitations, alternative approaches incorporating the use of an artificial magnetic conductor (AMC), substrate thinning technology, low back-etching (LBE), dielectric resonator antenna (DRA), inductor-capacitor loading, ion implantation, artificial dielectric layer (ADL), partial shield layers (PSL) and similar techniques have been demonstrated in the literature. The most adopted techniques are AMC, inductor-capacitor loading, PSL, and partially reflective surface (PRS) due to their cost-effectiveness and simple design configuration compared to the few mentioned.

* Corresponding author. E-mail address: eemfadzil@usm.my

English language proofreader: Yen-Chun Hsieh

Bean and Venkataraman [13] employed, an AMC to improve a gain of 60 GHz Yagi-Uda integrated OCA designed for short-range inter-chip communication. In the design, units of Jerusalem cross AMC were configured to achieve an increased gain of 11% and radiation efficiency of 12%. A study progressively demonstrated this technique, where AMC techniques have increased wideband, circular ring monopole integrated OCA performance [14]. The design considerably increased the operational gain, impedance bandwidth, and radiation efficiency. Similarly, the study employing AMC changes the performance of folded-dipole OCA by improving the antenna gain by 8 dB compared to the antenna without AMC [15]. Furthermore, inductance-capacitance loading [16] and PSL [17] represent another potential technique for enhancing OCA performance. These layers share similar characteristics with an AMC and PRS, and they equally aid in antenna miniaturization. For instance, a PSL was embedded within SiO_2 of 11 GHz meandered loop OCA, which yielded an increased gain of 4 dB, which is considered remarkable in OCA design [17].

However, an alternative technique for enhancing gain and radiation characteristics involves DRA loading, wherein a high-resistivity substrate would be added to the antenna, thereby mitigating losses associated with the lossy substrate. This method reduces surface wave generation and radiation loss by directing electromagnetic (EM) through a dielectric resonator before releasing them into the surrounding medium. Several studies have suggested using a DRA as an alternative approach. For example, Kong et al. [18] proposed a high gain, wide impedance bandwidth by incorporating a DRA into a low-profile OCA. The constructed prototype was tested, resulting in a radiation efficiency of 44% and an absolute gain of 8.6 dB. This method significantly performs as it reduces surface waves and loss attributed to metallization; besides, it faces integration challenges and incompatibility with modern complementary metal-oxide-semiconductor (CMOS) processes.

This study employs a PRS to enhance OCA performance, particularly the gain and radiation characteristics. PRS similarly behaves like AMC as it exhibits high impedance characteristics, where the magnitude of the surface impedance is based on the number of unit cells and the reactance parameters of the periodic structure [19]. The fundamental concept of artificially created surface or material is to achieve a high impedance surface (HIS) that acts as a whole or partial shield to the striking incidence wave on their surface, where both the PRS and AMC have such characteristics and consist of an array of unit cell or patch arranged periodically. They exhibit high-impedance properties and are engineered to reflect incoming waves with zero-phase shifts. However, while the PRS partially reflects incoming waves, directing them toward the lossy substrate, the AMC achieves high reflection. Its inclusion significantly improves the antenna gain and radiation efficiency over non-PRS-inspired designs. PRS enables partial reflection of incidence wave from confining into the lossy Si-substrate [20]. However, complete restriction of EM is not achievable as the CMOS metallization rule process limits the metal density usage to around 20-80% in both layers [3].

As OCA integration can be achieved by standard CMOS, Bi-CMOS process with metal-insulator-metal (MIM) configuration, or using SiO_2 on Si-wafer commonly using 250 μm, 500 μm, or 525μm based on metal-insulator-semiconductor (MIS) using CMOS design procedures. In this design, an MIS structure was used instead of standard CMOS process 0.18 μm or 0.13 μm technology due to the notable antenna performance, despite the significant feature of CMOS process 0.18 μm in chip design. To justify the importance of the adopted technology, the following reasons are enlisted based on the following parameters;

(1) Technology: In CMOS 0.18 μm technology, multiple layers of MIM are utilized to create an OCA, contrasting with just five layers of MIS used previously. This approach significantly enhances antenna performance compared to existing literature on 0.18 μm technology.
(2) Performance: Increasing the number of MIM layers in the configuration causes mutual coupling within the chip, which creates parasitic capacitance across the structure. This capacitance impacts the antenna's radiation resistance, pattern, and gain.

(3) Optimization: The CMOS technology fabricated using the standard 0.18 µm process is inherently inflexible compared to those built on 525 µm Si-wafers, which provide greater design flexibility and are easier to optimize at a lower fabrication cost, independent of manufacturer specifications.

(4) Cost: The 0.18 µm standard technology incorporates numerous reactive components and multiple metal layers, some dedicated to antenna design and others to different integration purposes. However, several layers remain unused, adding to power consumption and costs.

PRS offers distinct advantages over other mentioned techniques. For example, substrate loading and DRA incur additional integration costs and are incompatible with silicon substrates, while AMC increases metal density, leading to larger chip sizes and greater design complexity. On the other hand, substrate thinning and LBE require post-processing, resulting in high fabrication costs. PRS stands out with benefits such as low integration costs, the ability to enable multiple layer configurations within a small area, and a compact OCA design compared to other methods. However, PRS also has drawbacks, including partial reflection characteristics and susceptibility to significant changes in reflection and transmission coefficients, especially in high-frequency designs.

This paper is arranged as follows: the design and configuration of the proposed antenna, the periodic structure PRS design, and its characteristics are discussed in Section 2. In Section 3, the results and analysis of the simulated and corresponding measured parameters were discussed and presented. Thus, the results summary is concluded in Section 4.

2. Antenna Design and Analysis

This section covers the design and analysis of the proposed antenna and its configurations, including the geometric dimensions, materials, and tools used in the design process. Generally, the antenna features a multi-layered stacked structure with top metal as a radiator. The following section will provide a detailed presentation of the antenna parameters.

2.1. Antenna geometry and configuration

The proposed antenna geometrically follows the typical principles of CMOS design, wherein a six-layer MIS consists of SiO_2 layers, a ground conductor, PRS, a radiating element, and a silicon substrate [21-22]. The host material used was a processed silicon wafer of dielectric constant (ε_r) of 11.7-11.9 [6], a resistivity of 1-20 Ω-cm, and a thickness of 525 µm [6] coplanar waveguide (CPW) port is used as a feeding port due to its low profile, low dispersion, and integration simplicity [23], which is coupled to the monopole antenna (M1) on the top metal layer of the chip as depicted in Fig. 1.

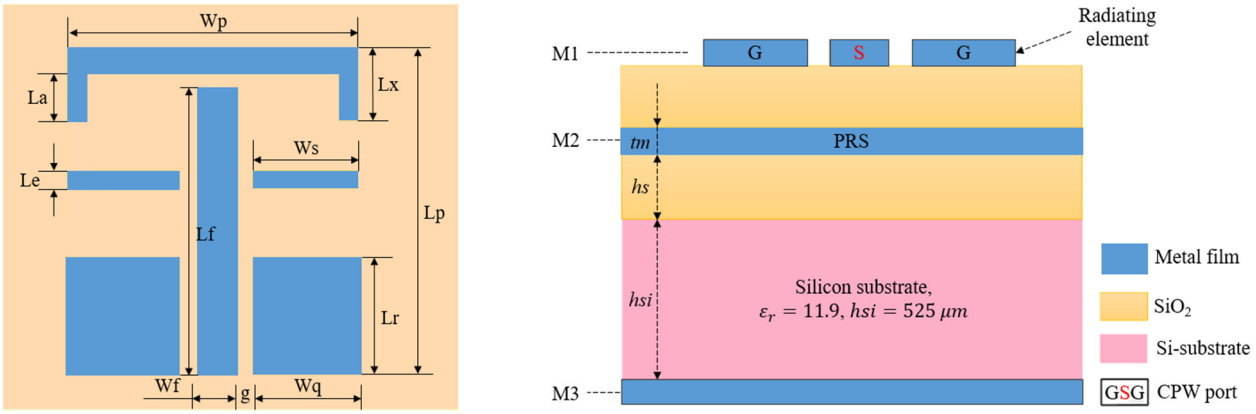

(a) Top view (b) Layered view

Fig. 1 Geometry of the proposed antenna

The design incorporates a PRS as a high-impedance surface (HIS). The radiator optimized to a dimension of 0.26 λ × 0.34 λ mm^2 fitted to be integrated as the OCA. Fig. 2(a) illustrates the stacked antenna structure showing two SiO_2 layers of 2.5 µm each, a thin film of silver material, and M1 of 1.7 µm were configured as insulators and the radiating conductor. The

second metallization (M2) is used as the PRS and embedded within the layers of SiO_2 as a reflective surface, which acts as a shield to the confining EM wave migrating from the radiating element into the lossy Si-substrate. The third metallization (M3) is the ground plane of the chip. An optimized dimension of the radiating element is shown in Table 1.

Table 1 Optimized parameters of the proposed antenna

Parameter	Value (mm)	Parameter	Value (mm)
Le	1.0	Wf	2.0
Ws	5.45	Lp	17.62
Lx	5.62	La	4.12
Wq	5.45	Lr	5.7
Wp	13.91	Lf	15.4
tm	0.001	hs	0.002
hsi	0.525	g	0.505

2.2. *Design of partially reflective surface*

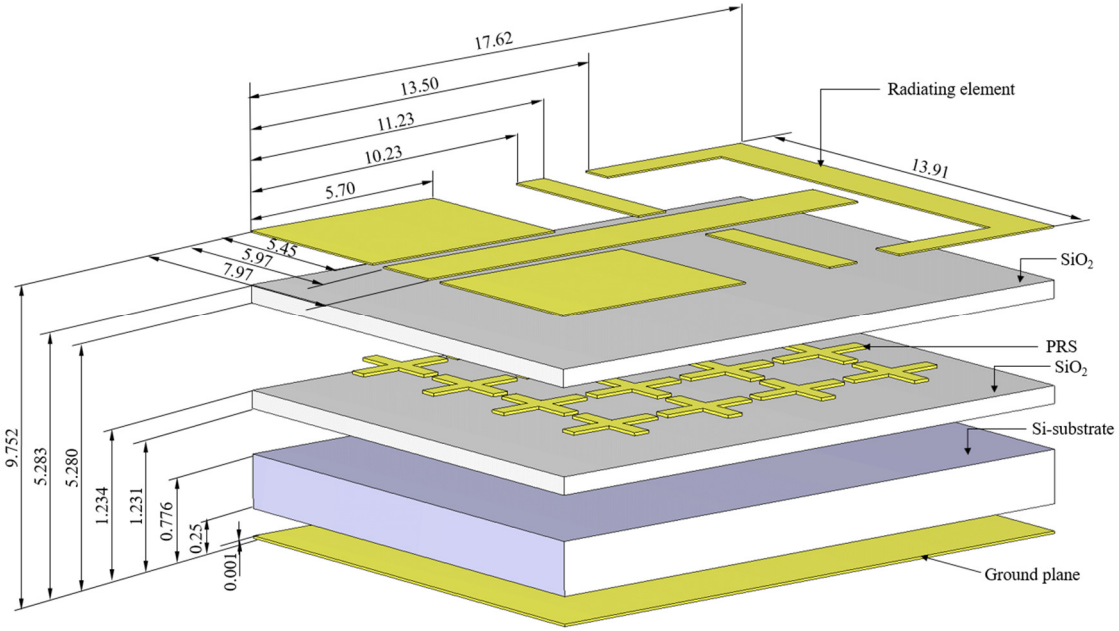

(a) Isometric stacked-up view

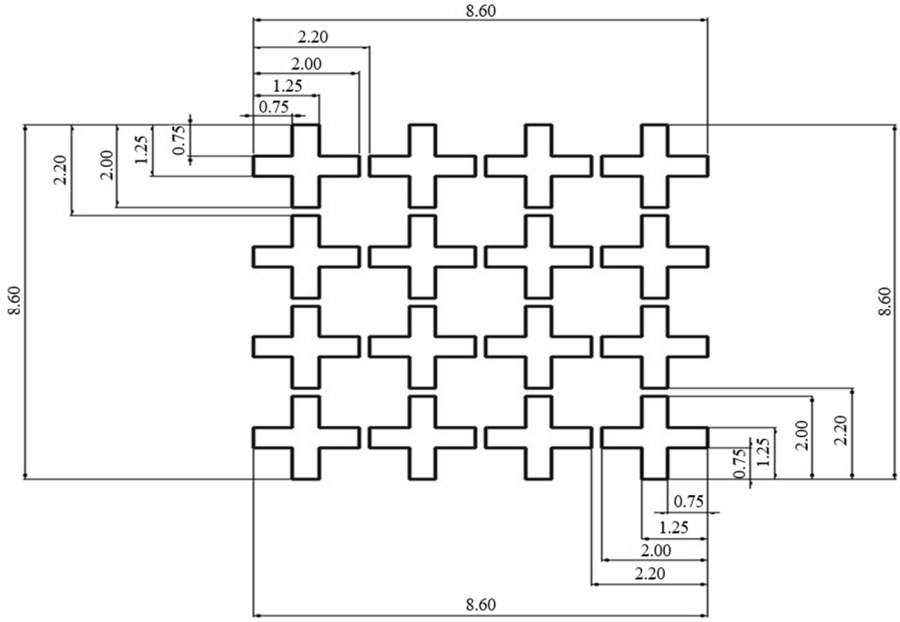

(b) Periodic PRS structure

Fig. 2 Staked up layers of the proposed design

PRS is the arrangement of regular metal film designed to be HIS embedded between the layers of SiO_2. It has working features similar to an AMC. PRS acts to obstruct migrated incidence power from the radiating element to the lossy Si-substrate. It can be designed to plump the magnitude of the reflected signal and control the antenna's resonance [19]. For example, in CMOS process design, embedding a high impedance periodic structure within the layers of SiO_2 restricts a reflected incidence wave emanating from the radiator toward the Si-substrate [24], thereby minimizing the power losses of the OCA. In this design, a periodic aperture of 4 × 4 unit cells of metal thickness, t_m = 1 μm, a length and width of a = 2 mm each configured as an aperture of HIS. The structure is embedded into the thin SiO_2 layers shown in Fig. 2(b).

2.3. *Characteristics of PRS structure*

A single unit of the PRS was configured and positioned within the waveguide ports with boundary conditions set at the x-plane and y-plane and simulated using a frequency domain solver. Consequently, in Fig. 3(a), the reflection and transmission coefficients of the structure are depicted, while Fig. 3(b) showcases the reflection phase at 5.804 GHz. The characteristic response of Fig. 3(a) indicates that the peak reflection coefficient occurred below -0.19 dB and the reflection coefficient at -24.1 dB across a bandwidth of 5.68-5.92 GHz.

Similarly, Fig. 3(b) illustrates a zero-degree reflection phase at 5.88 GHz with a slight shift in the center frequency of 5.8 GHz. This indicates that the incident wave was hindered due to the high impedance generated by the PRS. Moreover, it resulted in an insertion loss of about 3 dB at the transmission phase from 5.62 GHz at the lower side frequency and 6.16 GHz at the upper side frequency with 5.804 GHz as the center frequency.

2.4. *Effect of PRS patch separation distance on the reflection phase*

The characteristics of the PRS indicate that the reflection phase magnitude is influenced by the number of unit cells or patches, the spacing between the patches, and their thickness. This section examined the PRS's effectiveness based on the separation gap, s, between adjacent patches, which indirectly reduces the length and width of the patch. The optimized PRS patch size and gap are 2 mm and 0.2 mm, respectively. Consequently, a parametric analysis of the separation, s, was conducted from 1.5 mm to 3 mm in 0.5 mm intervals.

Fig. 3(c) illustrates the impact of the gap between PRS patches on the reflection phase magnitude. The plots reveal that the magnitude of the reflection phase decreases as the separation gap increases. This is due to the additional change in capacitance between adjacent patches, as the capacitance between two adjoining patches is inversely proportional to the separation distance. This change in capacitance significantly affects the reflection phase antenna's performance.

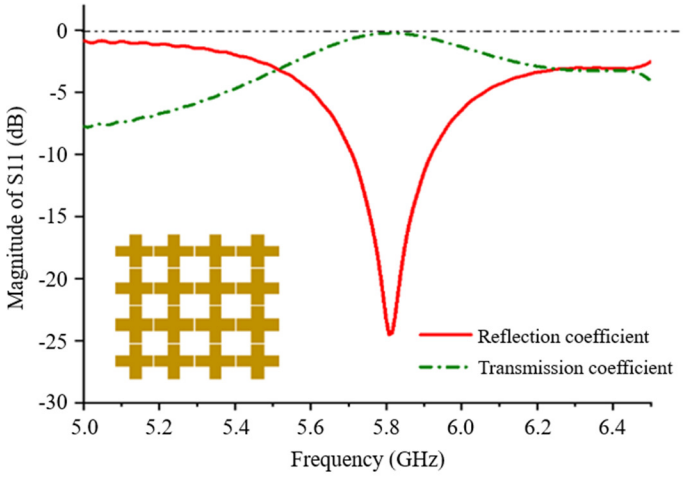

(a) Reflection and transmission

Fig. 3 The simulated coefficients and the reflection phase of PRS at 5.8 GHz

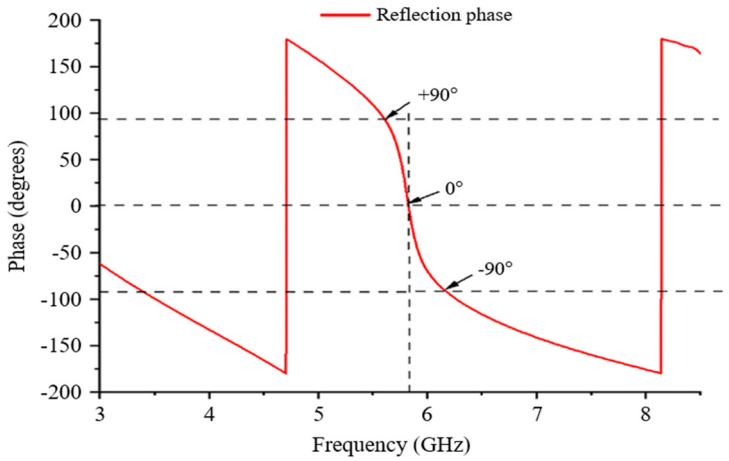

(b) Reflection phase

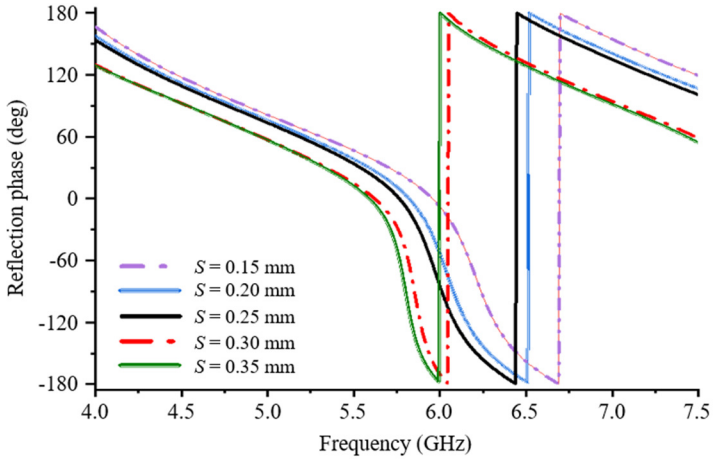

(c) Effect of SiO_2 thickness on the antenna gain

Fig. 3 The simulated coefficients and the reflection phase of PRS at 5.8 GHz (continued)

3. Measured Results and Analysis

Measurement is a crucial phase for evaluating the simulation results. It outlines the comprehensive analysis of the results obtained, as well as the procedures and graphical presentation of the results. In this design, detailed measurements of the fabrication process, measurement procedures, and equipment are included. The primary measured parameters include the return loss, gain, radiation efficiency, radiation pattern, and antenna impedance bandwidth.

3.1. Antenna fabrication process

Prototype development of the design was realized based on the CMOS compatibility procedure, where direct current (DC) sputtering and chemical vapor deposition (CVD) technologies were employed. A processed standard Si-substrate, p-type, 100 orientations, 525 μm thick, and resistivity of 1-20 Ω-cm was selected to accomplish the process. The stacked structure consists of thin layers of SiO_2, top metal (M1), PRS (M2), and ground conductor (M3), all stacked on the substrate to form a single structure.

Step 1, a thin layer of 1 μm of silver (Ag) material was deposited at the bottom of the Si-substrate, which acts as a ground conductor.

Step 2, a CVD process was used to deposit a 2.5 μm SiO_2 layer on top of the Si-substrate as an insulation segment. The Step 1 was repeated for depositing PRS (M2) of 1 μm thickness. Similarly, the second SiO_2 layer was deposited on top of the PRS layer utilizing the same process as Step 2.

Finally, the monopole planar radiator (M1) of 1 µm was deposited on the top metal layer on the upper layer. Fig. 4(a) and 4(b) show the fabrication process and final fabricated prototype, while Fig. 4(c) depicts the measurement set-up.

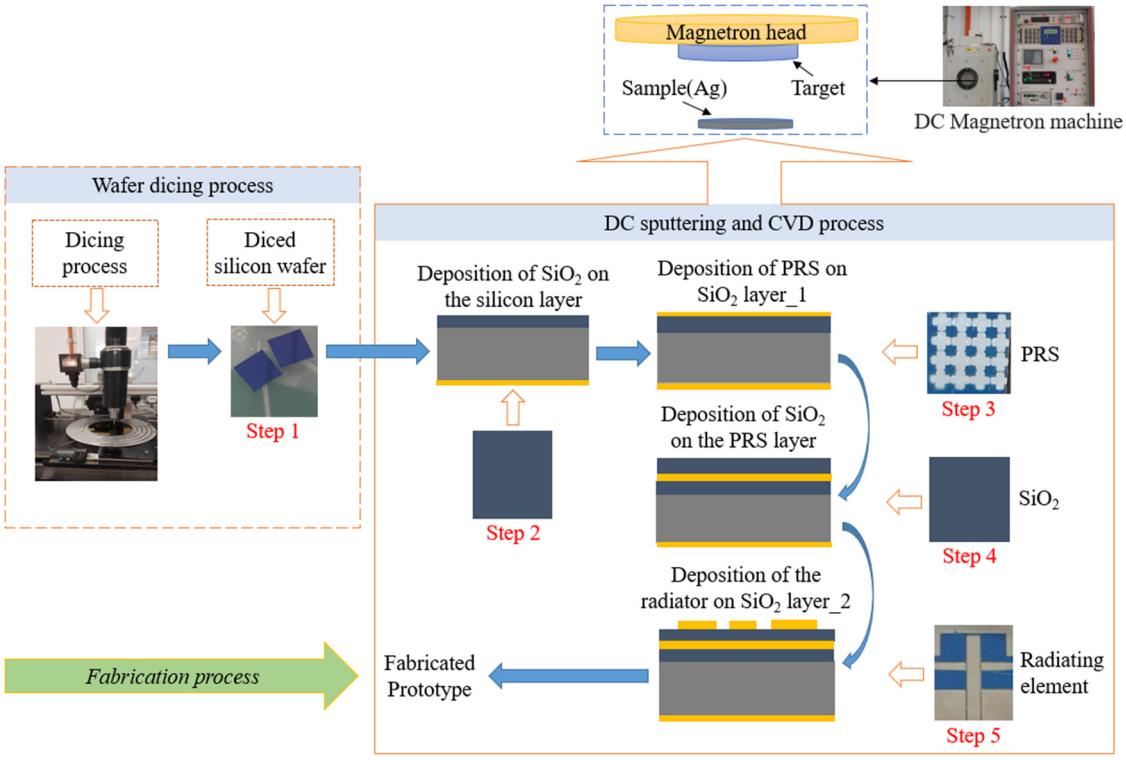

(a) Fabrication process

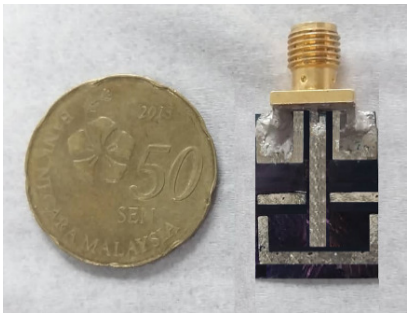

(b) Fabricated prototype

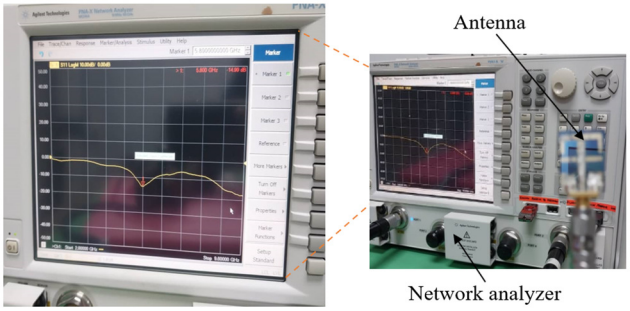

(c) Measurement set-up

Fig. 4 Fabrication and measurement set-up of the proposed antenna

3.2. Impedance, radiation characteristics, gain and efficiency

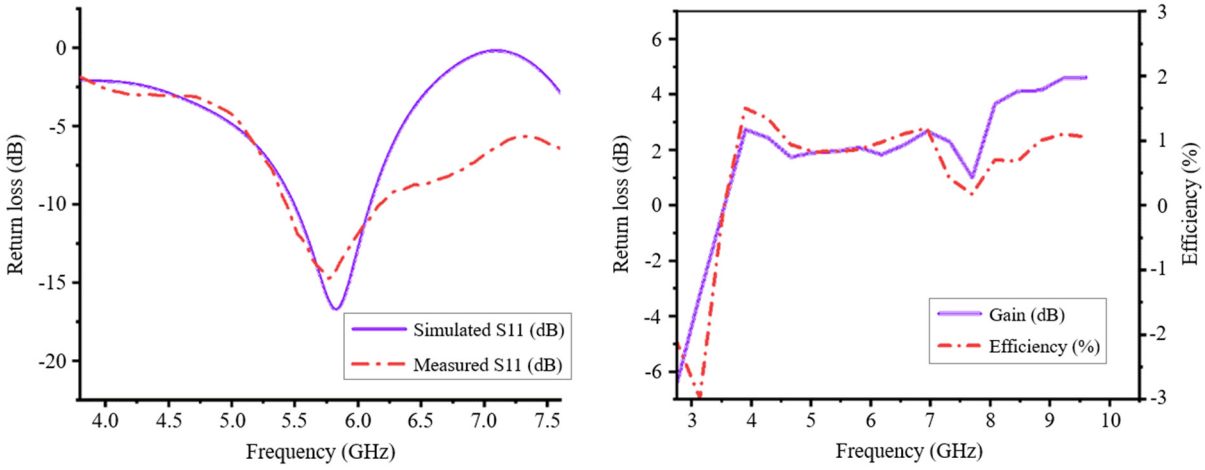

(a) Simulated and measured return loss

(b) Gain and Efficiency

Fig. 5 Simulated and measured parameters of the proposed at 5.8 GHz

Following the fabrication process, this section presents the measured performance of the proposed antenna, introducing the reflective surface, PRS, which significantly enhanced the antenna's gain and radiation efficiency. Specifically, compared to the antenna without PRS, the antenna achieved a notable increase in gain of 24.3% and efficiency of 16.25%. Notably, a significant agreement is observed between the simulated and measured parameters. The fabricated prototype was measured and realized a maximum gain of 2.14 dB with a radiation efficiency of 72.2%, as shown in Fig. 5. Although minor discrepancies in antenna parameters were noted, likely due to mismatches and fabrication tolerances.

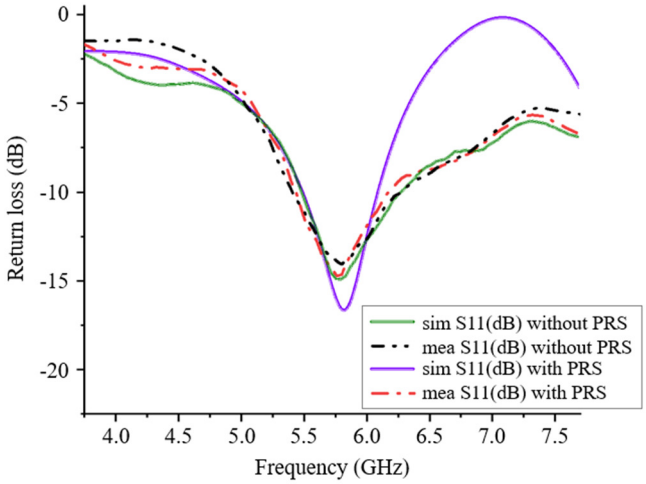

(a) Magnitude of S11 (dB)

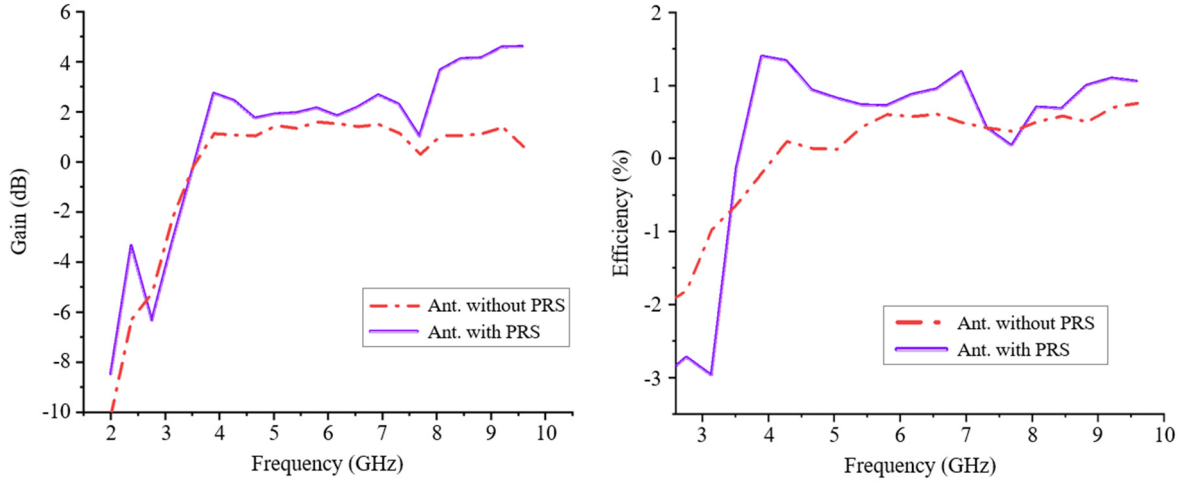

(b) Gain (dB) (c) Efficiency (%)

Fig. 6 The comparison S11, gain and efficiency of an antenna with and without PRS

Moreover, efficiency is measured based on the gain and directivity derived from characteristic measurements. Initially, these values were determined by setting an Agilent signal generator 83640B to 0 dBm and an operating frequency of 5.8 GHz. The output power was recorded using a network signal analyzer N9030A, which was connected to a receiver antenna positioned at a distance S from the transmitter antenna, as illustrated in Fig. 6. A broadband horn antenna (LB-20200-SF) with a gain of 20 dB and a frequency range of 2-20 GHz served as the transmitter antenna. Measurements were repeated at various values of S until the maximum gain was identified. A link budget based on Friis's transmission formula below was employed to calculate the maximum gain in dB. Consequently, peak gains of 1.587 dB and 2.138 dB were achieved for the antenna under test (AUT) with and without PRS, respectively.

$$P_r = P_t + G_t + G_r + L_p - P_{cl} \tag{1}$$

$$G = \frac{2\pi d}{\lambda}\sqrt{\frac{P_r}{P_t}}\ (\text{mW}) \tag{2}$$

$$G = 10\log_{10}\left(\frac{2\pi d}{\lambda}\sqrt{\frac{P_r}{P_t}}\right) \text{ (dB)} \tag{3}$$

where, P_t and P_r are the transmitted power by the transmitter and received power by the receiver (dBm), G_t and G_r are the gain of the transmitter antenna, and the receiver antenna's gain (dB). P_{cl} and L_p are cable loss (dBm) and the loss due to free space. Hence, L_p can be determined as:

$$L_p = 34.21 + 20\log s + 20\log f \tag{4}$$

$$s \geq \frac{2d^2}{\lambda} \tag{5}$$

The performance of the antenna with and without the PRS was compared in terms of S11, gain, and efficiency, as illustrated in Fig. 6. The 2D radiation characteristic of the model in the E-plane and H-plane were plotted as shown in Fig. 7, where s is the distance between the transmitter and receiver antenna, d is the diameter of the horn antenna, λ is the wavelength, and f is the operating frequency in (MHz).

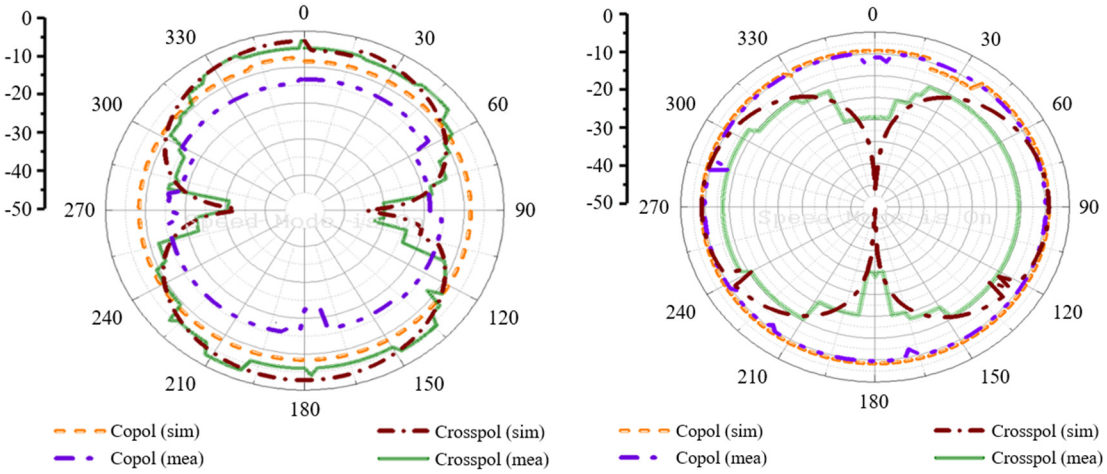

(a) E-plane (b) H-plane

Fig. 7 Simulated and measured 2D radiation pattern at 5.8 GHz

In a similar procedure, the directivity of the AUT was assessed based on the measured radiation pattern, where the gain and the corresponding theta (degree) for the E-plane and H-plane were plotted on a polar graph, and the equivalent half-power beam width (HPBW) angle denoted as θ^E and θ^H were measured. The directivity was then determined as:

$$D = \frac{32400}{\theta^E \times \theta^H} \tag{6}$$

$$\eta = \frac{P_r}{P_r + P_L} \tag{7}$$

$$\eta = \frac{G}{D} \tag{8}$$

Subsequently, Eqs. (7) and (8) were used to measure the radiation efficiency of the antenna. However, the result for Eq. (8) was finally chosen for accuracy, considering the relationship between gain, directivity, and losses incurred by antenna components such as dielectric and conductor tied to antenna design material. This equation also aligns with IEEE standards for calculating radiation efficiency.

To assess the notable impact of the similarity in pattern between the simulated and measured characteristics. However, some variation exists ascribed to unavoidable path loss, conductor loss, interference, and stacking tolerance due to the metallic layers. This positive implementation underscores the efficacy of the design modifications in improving antenna performance.

However, the impact of the PRS on the reflection coefficient was noted by positioning it at various separation distances (d) from the upper antenna element. This led to a frequency shift caused by induced mutual coupling and parasitic capacitance across the region, as depicted in Fig. 8. Equally, significant values for the gain, radiation efficiency, and bandwidth below a return loss below -10 dB were achieved. The simulation outcomes indicated an impedance bandwidth of 0.72 GHz, which is 5.56% greater than the measured bandwidth of 0.68 GHz. Consequently, this bandwidth aligns well with the requirements of Wi-Fi, WiMAX, and RFIC applications at 5.8 GHz [25].

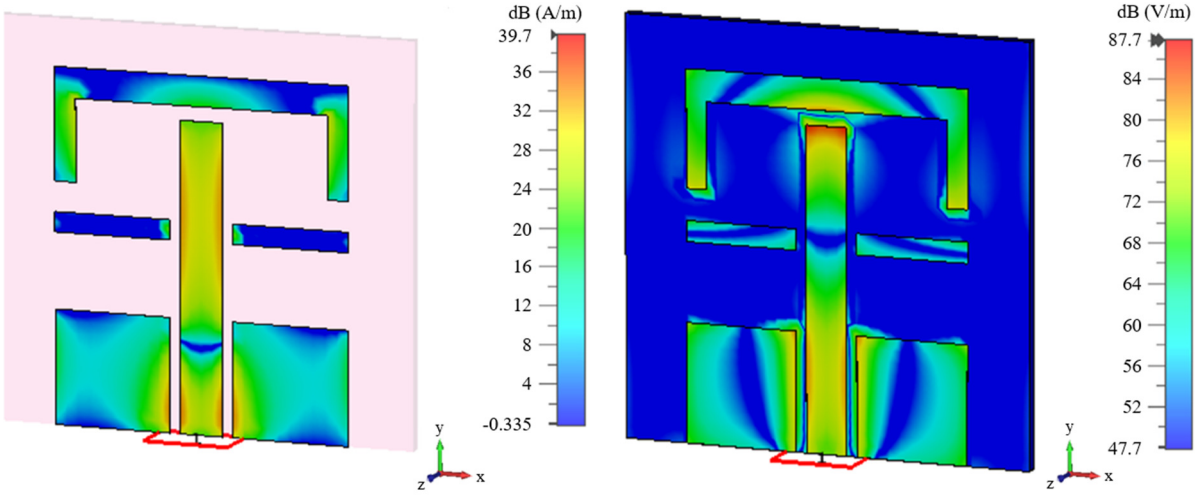

(a) Surface current distribution (b) E-field

Fig. 8 Simulated surface and E-field at 5.8 GHz

3.3. *Surface current distribution and E-field vector*

Due to the varied characteristics of the antenna radiation pattern, the antenna's surface current distribution and electric field (E-field) were also analyzed. Figs. 8(a) and 8(b) illustrate the E-field strength and surface current distribution at 5.8 GHz. As shown in Fig. 8(a), the E-field concentration is highest at the excitation port and along the entire signal conductor, while it is lower at the antenna's curvature. Similarly, the surface current distribution is most significant around the excitation point and along the center conductor, with less distribution observed in other parts of the antenna. The increased surface current distribution along the metallic path enhances the antenna's radiation characteristics, indicating that the strength of the current distribution effectively transforms the transverse electromagnetic (TEM) mode near the port into a parallel plate mode.

3.4. *Effect of PRS separation distance on the reflection coefficient*

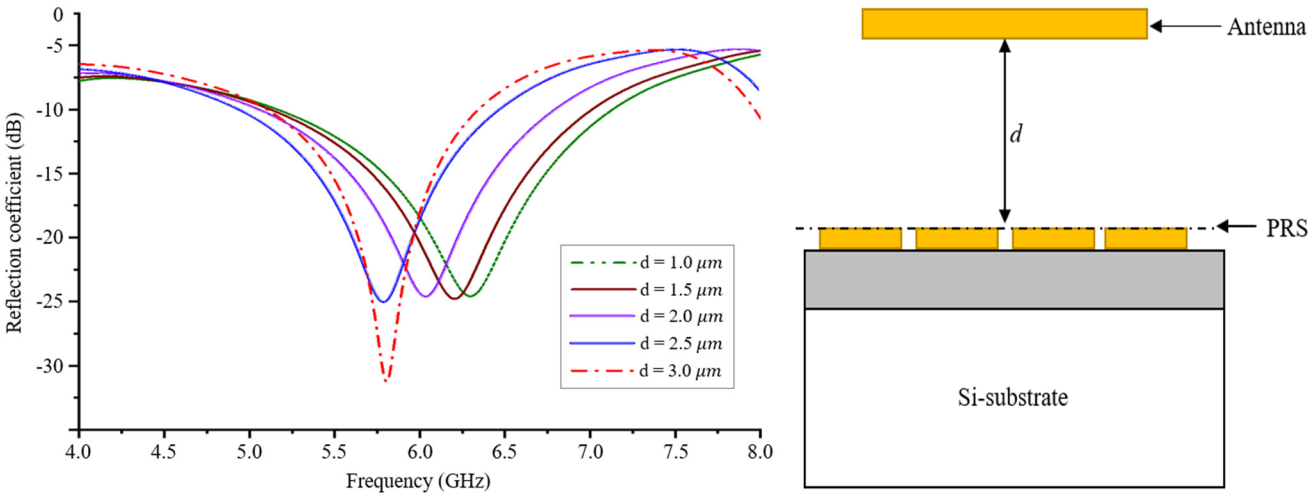

(a) Frequency vs. reflection coefficient (b) Antenna-PRS model

Fig. 9 Effect of PRS separation on the reflection coefficient

This section investigated the effect of the separation distance between the PRS and the top antenna element. The antenna is positioned above the PRS structure, and the impact of the separation distance between the antenna and PRS, denoted as *d*, is investigated. Distances *d* from 1 μm to 3 μm at 0.5 μm intervals are considered. A SiO_2 with a permittivity of 3.8 is utilized between the PRS and the antenna. Fig. 9 shows the simulation outcomes, revealing a noticeable shift in resonance frequency as the separation distance increases, where d equals 2.5 μm and 3 μm corresponds to the target frequency of 5.8 GHz. This shift is attributed to the mutual coupling between the PRS and the top radiating element, leading to the induction of parasitic capacitance across the separation. Thus, it is evident that altering the capacitance values, whether increasing or decreasing them, significantly affects the resonance frequency as it is inversely proportional to the equivalent capacitance. Which can be expressed as;

$$F_R \alpha \frac{1}{\sqrt{C_{eq}}} \tag{9}$$

where C_{eq} is an equivalent capacitance between the separation, and the F_R is the antenna's resonant frequency. However, To achieve PRS's height optimization, the following factors should be considered: ensuring that the reflected phase is within -90° to +90°. This means that the PRS's operating frequency should equal the desired frequency.

$$f_{dev} = \left| f_c - f_m \right| \tag{10}$$

$$f_{band} = \left| f_{max} - f_{min} \right| \tag{11}$$

Secondly, the bandwidth of the structure is as wide as possible in such a deviation in frequency, f_{dev} is minimized, and band frequency, f_{band} is maximized as expressed in:

$$f = \left[maximize\left(f_{band} \right), minimize\left(f_{dev} \right) \right] \tag{12}$$

Secondly, when optimizing the PRS height, it's crucial to account for the distance between the PRS and the radiating conductor to prevent the incidence and reflected waves from overlapping in time, as given in:

$$\varphi_{PRS}(f) = \varphi_r(f) - \varphi_{inc}(f) + \frac{4\pi fd}{v} \tag{13}$$

where *f* is the frequency (Hz), $\varphi_{PRS}(f)$ is the PRS shift in the reflection phase, $\varphi_r(f)$ is the reflected wave phase, $\varphi_{inc}(f)$ is the incidence wave phase, *d* denotes the distance between the PRS and the top antenna, and *v* is the speed of the medium. However, f_c is the center frequency at 0° reflection phase, f_m is the medium frequency obtained at 0° reflection phase, and f_{min} and f_{max} are bandwidth minimum and maximum frequency.

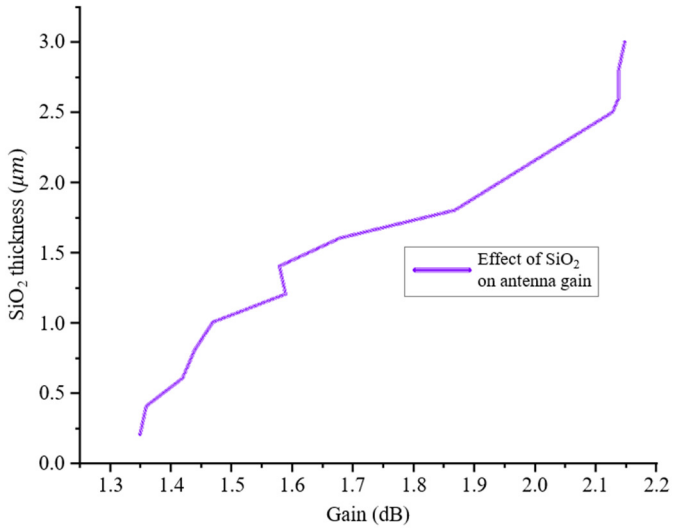

Fig. 10 Parametric studies on the effect of SiO_2 on the antenna gain

3.5. A parametric analysis of the effect of PRS geometry on the reflection phase

In the OCA structure, comprising SiO_2, metal layers, and a lossy Si-substrate, previous studies and this research highlight the critical role of the insulation layer, SiO_2, in shaping antenna performance. Minor changes in SiO_2 thickness significantly impact both gain and radiation resistance by providing insulation between the metallization layers and the Si-substrate. The parametric analysis shows that increasing SiO_2 thickness widens the separation between the PRS and the Si-substrate and between the PRS and the top antenna element. This results in a notable gain enhancement. Fig. 10 illustrates the effect of varying SiO_2 on antenna gain.

3.6. Comparative analysis of the proposed antenna and the performance of published work

Table 2 compares the proposed design's performance and other OCAs, focusing on gain, radiation efficiency, bandwidth, and technology. This work utilized MIS components following the metallization rule of the CMOS process, employing only three metal layers to reduce the fabrication and material cost. Despite the few metal layers, the proposed antenna achieved a gain of 2.14 dB and a radiation efficiency of 72.2%. This improvement is attributed to the reduced dielectric losses and magnetic coupling across the layers. In contrast, previous work utilized standard CMOS technology 0.18 μm and 0.13 μm. Although OCA design using these technologies is notably compact, facilitating integration into smaller chip sizes. However, this results in a low gain and radiation efficiency, significantly reducing the antenna's performance. The proposed OCA facilitates a physical connection to the coaxial port of 50 Ω and simplifies real-time measurement as no micrograph technology is required. Thus, integration into the transceiver is achievable by replacing the port and utilizing the CPW pad to enable connection to the front-end circuit.

Table 2 Comparison of the proposed antenna with previous literature

Ref	Antenna type	Freq (GHz)	Size (λ^2)	Max gain (dB)	Rad. Eff (%)	Return loss (dB)	Technology
[17]	Monopole meandered	9.45	0.063 × 0.066	-29.2	21.07	13.2	0.18 μm CMOS
[22]	Meander loop	5.8	0.12 × 0.01	-40	25	NM	0.13 μm CMOS
[25]	Loop	5.8	0.027 × 0.027	-48.93	NM	48.09	0.18 μm CMOS
[26]	Meander dipole	2.4	0.032 × 0.032	-23.8 (in Air) -25.9 (in skin)	60	<-10	0.18 μm CMOS
[27]	Loop	5.8	0.020 × 0.016	-23.7	NM	-	0.18 μm CMOS
[28]	Folded dipole	5.8	0.079 × 0.77	2.1	68.7	-23	MIS-Si-wafer
[29]	Folded loop	2.4	0.012 × 0.012	-20.8	31.2	NM	UMC 0.18 μm
This work	Monopole planar	5.8	0.26 × 0.34	2.14	72.2	14.99	0.525μm Si wafer + SiO_2

4. Conclusion

This article introduces a monopole planar OCA with improved gain and radiation performance. A six-layer MIS stacked structure was configured as the OCA. The design incorporates a PRS aperture as the gain and radiation enhancement technique. A DC magnetron sputtering and CVD technologies were employed for the prototype development. The prototype was measured and obtained an increased gain of 24.3%, elevating it from 1.59 dB to 2.14 dB, yielding a peak radiation efficiency of 72.2%. This broadened the measured impedance bandwidth of the antenna to 0.63 GHz, covering the range from 5.56 GHz to 6.24 GHz.

The radiation characteristics of the prototype were assessed, revealing a similar radiation pattern in both absolute measured and simulated plots. This indicates a consistent alignment between the simulated and measured patterns. However, minor discrepancies and irregularities were noted in the measured radiation patterns, attributed to fabrication tolerances and

reactance generated across layers due to utilizing multiple components with varying dielectric properties. Despite these variations, the prototype exhibited desirable bandwidth, gain, and efficiency, enabling its integration with RF front-end circuitry, RFIC, and WiMax at 5.8 GHz despite the larger wavelength at a lower frequency.

Acknowledgment

This work was supported by the Ministry of Higher Education Malaysia through the Fundamental Research Grant Scheme under FRGS/1/2023/TKO7/USM/01/1.

Conflicts of Interest

The authors declare no conflict of interest.

References

[1] Q. H. Abbasi, S. F. Jilani, A. Alomainy, and M. A. Imran, Antennas and Propagation for 5G and Beyond, Herts, United Kingdom: The Institution of Engineering and Technology, pp. 123-155, 2020.

[2] R. Karim, A. Iftikhar, B. Ijaz, and I. Ben Mabrouk, "The Potentials, Challenges, and Future Directions of On-Chip-Antennas for Emerging Wireless Applications—A Comprehensive Survey," IEEE Access, vol. 7, pp. 173897-173934, 2019.

[3] M. A. Rossi, "The Advent of 5G and the Non-Discrimination Principle," Telecommunications Policy, vol. 46, no. 4, article no. 102279, May 2022.

[4] H. M. Cheema and A. Shamim, "The Last Barrier: On-Chip Antennas," IEEE Microwave Magazine, vol. 14, no. 1, pp. 79-91, January-February 2013.

[5] N. O. Parchin, M. Alibakhshikenari, H. J. Basherlou, R. A. Abd-Alhameed, J. Rodriguez, and E. Limiti, "MM-Wave Phased Array Quasi-Yagi Antenna for the Upcoming 5G Cellular Communications," Applied Sciences, vol. 9, no. 5, article no. 978, March 2019.

[6] W. A. Ahmad, M. Kucharski, A. Di Serio, H. J. Ng, C. Waldschmidt, and D. Kissinger, "Planar Highly Efficient High-Gain 165 GHz On-Chip Antennas for Integrated Radar Sensors," IEEE Antennas and Wireless Propagation Letters, vol. 18, no. 11, pp. 2429-2433, November 2019.

[7] Y. P. Zhang and D. Liu, "Antenna-on-Chip and Antenna-in-Package Solutions to Highly Integrated Millimeter-Wave Devices for Wireless Communications," IEEE Transactions on Antennas and Propagation, vol. 57, no. 10, pp. 2830-2841, October 2009.

[8] B. Sene, D. Reiter, H. Knapp, and N. Pohl, "Design of a Cost-Efficient Monostatic Radar Sensor With Antenna on Chip and Lens in Package," IEEE Transactions on Microwave Theory and Techniques, vol. 70, no. 1, pp. 502-512, January 2022.

[9] Y. Zhang, "Antenna-in-Package (AiP) Technology," Engineering, vol. 11, pp. 18-20, April 2022.

[10] R. Karim, A. Iftikhar, and R. Ramzan, "Performance-Issues-Mitigation-Techniques for On-Chip-Antennas – Recent Developments in RF, MM-Wave, and Thz Bands With Future Directions," IEEE Access, vol. 8, pp. 219577-219610, 2020.

[11] M. R. Karim, X. Yang, and M. F. Shafique, "On-Chip Antenna Measurement: A Survey of Challenges and Recent Trends," IEEE Access, vol. 6, pp. 20320-20333, 2018.

[12] Q. Liu, A. J. van den Biggelaar, U. Johannsen, M. C. van Beurden, and A. B. Smolders, "On-Chip Metal Tiling for Improving Grounded MM-Wave Antenna-On-Chip Performance in Standard Low-Cost Packaging," IEEE Transactions on Antennas and Propagation, vol. 68, no. 4, pp. 2638-2645, April 2020.

[13] D. Bean and J. Venkataraman, "Gain Enhancement of On-Chip Antenna at 60 GHz Using an Artificial Magnetic Conductor," IEEE International Symposium on Antennas and Propagation and North American Radio Science Meeting, pp. 1423-1424, July 2020.

[14] H. T. Huang, B. Yuan, X. H. Zhang, Z. F. Hu, and G. Q. Luo, "A Circular Ring-Shape Monopole On-Chip Antenna With Artificial Magnetic Conductor," Asia-Pacific Microwave Conference, pp. 1-3, December 2015.

[15] M. Nafe, A. Syed, and A. Shamim, "Gain-Enhanced On-Chip Folded Dipole Antenna Utilizing Artificial Magnetic Conductor at 94 GHz," IEEE Antennas and Wireless Propagation Letters, vol. 16, pp. 2844-2847, 2017.

[16] K. Okabe, W. Lee, Y. Harada, and M. Ishida, "Silicon Based On-Chip Antenna Using an LC Resonator for Near-Field RF Systems," Solid-State Electronics, vol. 67, no. 1, pp. 100-104, January 2012.
[17] H. Singh and S. K. Mandal, "Miniaturized On-Chip Meandered Loop Antenna With Improved Gain Using Partially Shield Layer," 14th European Conference on Antennas and Propagation, pp. 1-4, March 2020.
[18] S. Kong, K. M. Shum, C. Yang, L. Gao and C. H. Chan, "Wide Impedance-Bandwidth and Gain-Bandwidth Terahertz On-Chip Antenna With Chip-Integrated Dielectric Resonator," IEEE Transactions on Antennas and Propagation, vol. 69, no. 8, pp. 4269-4278, August 2021.
[19] C. C. Liu and R. G. Rojas, "V-Band Integrated On-Chip Antenna Implemented With a Partially Reflective Surface in Standard 0.13- μm BiCMOS Technology," IEEE Transactions on Antennas and Propagation, vol. 64, no. 12, pp. 5102-5109, December 2016.
[20] A. V. Mamishev, K. Sundara-Rajan, F. Yang, Y. Du, and M. Zahn, "Interdigital Sensors and Transducers," Proceedings of the IEEE, vol. 92, no. 5, pp. 808-845, May 2004.
[21] R. K. Kushwaha, P. Karuppanan, and R. K. Dewang, "Design of a SIW On-Chip Antenna Using 0.18-μm CMOS Process Technology at 0.4 THz," Optik, vol. 223, article no. 165509, December 2020.
[22] J. J. Lin, H. T. Wu, Y. Su, L. Gao, A. Sugavanam, J. E. Brewer, et al., "Communication Using Antennas Fabricated in Silicon Integrated Circuits," IEEE Journal of Solid-State Circuits, vol. 42, no. 8, pp. 1678-1687, August 2007.
[23] S. Peddakrishna, L. Wang, V. Kollipara, and J. Kumar, "Compact Circularly Polarized Monopole Antenna Using Characteristic Mode Analysis," Proceedings of Engineering and Technology Innovation, vol. 24, pp. 1-14, April 2023.
[24] A. P. Feresidis, G. Goussetis, S. Wang, and J. C. Vardaxoglou, "Artificial Magnetic Conductor Surfaces and Their Application to Low-Profile High-Gain Planar Antennas," IEEE Transactions on Antennas and Propagation, vol. 53, no. 1, pp. 209-215, January 2005.
[25] A. H. A. Razak, M. I. A. Shamsuddin, M. F. M. Idros, A. K. Halim, A. Ahmad, and S. A. M. Al Junid, "Design of 5.8 GHz Integrated Antenna on 180nm Complementary Metal Oxide Semiconductor (CMOS) Technology," IOP Conference Series: Materials Science and Engineering, vol. 341, article no. 012015, 2018.
[26] A. Ray, A. De, and T. K. Bhattacharyya, "A Package-Cognizant CMOS On-Chip Antenna for 2.4 GHz Free-Space and Implantable Applications," IEEE Transactions on Antennas and Propagation, vol. 69, no. 11, pp. 7355-7363, November 2021.
[27] E. Charlot, M. Hamada, and T. Kuroda, "An On-Chip Antenna With an Area of 0.9 Square Millimeters for RFID Applications in the 5.8 GHz – 24 GHz Range," International Symposium on Antennas and Propagation, pp. 41-42, January 2021.
[28] A. Girgiri, M. F. Ain, B. A. Muhammad, and A. S. Mohammed, "Design of Miniaturized Folded Dipole Integrated On-Chip Antenna for 5.8GHz Application," IEEE International Symposium On Antennas and Propagation, pp. 1-2, October-November 2023.
[29] S. Archana and M. Bhaskar, "An Integrated 2.4 GHz Inductorless Power Amplifier and On-Chip Two Turn Folded Loop Antenna for Biotelemetry Applications," 14th International Conference on Computing Communication and Networking Technologies, pp. 1-6, July 2023.